Hindawi
Advances in Materials Science and Engineering
Volume 2017, Article ID 3701740, 15 pages
https://doi.org/10.1155/2017/3701740

Research Article

Impact of Cyclic Loading on Chloride Diffusivity and Mechanical Performance of RC Beams under Seawater Corrosion

Sen Pang,[1] Bo Diao,[1,2] Yinghua Ye,[1] Shuxin Chen,[1] and Xin Wang[1]

[1]*School of Transportation Science and Engineering, Beihang University, Beijing 100191, China*
[2]*State Laboratory of Subtropical Building Science, South China University of Technology, Guangzhou 510640, China*

Correspondence should be addressed to Yinghua Ye; yhye@buaa.edu.cn

Received 24 March 2017; Accepted 19 June 2017; Published 10 August 2017

Academic Editor: Xiao-Yong Wang

An experimental study was conducted to investigate the impact of cyclic loading on the mechanical performance and chloride diffusivity of RC beams exposed to seawater wet-dry cycles. To induce initial damage to RC beam specimen, cyclic loading controlled by max load and cycles was applied. Then beam specimens underwent 240 wet-dry cycles of seawater. Results show that the chloride content increased as max load and cycle increased. The chloride content at steel surface increased approximatively linearly as average crack width increased. Moreover, the max load had more influence on chloride content at steel surface than cycle. The difference of average chloride diffusion coefficient between tension and compression concrete was little at uncracked position. Average chloride diffusion coefficient increased as crack width increased when crack width was less than 0.11 mm whereas the increasing tendency was weak when crack width exceeded 0.11 mm. The residual yield load and ultimate load of RC beams decreased as max load and cycle increased. Based on univariate analysis of variance, the max load had more adverse effect on yield load and ultimate load than cycle.

1. Introduction

Reinforced concrete (RC) structures in coastal environment are damaged by service load and seawater erosion. Chloride ion penetrates into concrete through cracks, which causes steel corrosion. RC structures in coastal environment suffer compound action of service load and corrosion environment, leading to quick degradation of mechanical performance. In previous work (Rodriguez and Hooton [1]; Şahmaran [2]; Bentz et al. [3]; Jang et al. [4]), the correlativity between crack width of concrete and chloride diffusion coefficient was studied. The study of Wang and Zhang [5] presented a numerical procedure to simulate chloride ingression into cracked concrete with different crack geometry characteristics. The results showed that, with the increasing of crack width, crack depth, and crack amount, chloride ingression would be aggravated. The chloride transmission in cracked concrete was studied by Li et al. [6] experimentally and numerically. Results showed that when the crack width was less than 0.05 mm, the influence of the crack could be neglected. When the crack width increased from 0.08 mm to 0.1 mm, the dispersion increased. When the crack width was larger than 0.1 mm, the chloride transmission was similar to that in the liquid. The chloride penetration depth from both specimen surface and crack surface was studied by Win et al. [7]. Results showed that the chloride penetration depth from the crack surface was equal to or slightly higher than that from specimen surface with ratio w/c of 0.45 and 0.65. In the study of Li [8, 9], the effect of crack width on chloride diffusion was investigated experimentally and crack width threshold 0.1 mm was proposed.

Many studies focused on the chloride diffusion model. Park et al. [10] considered binder hydration and curing ages and developed a numerical model to predict time-dependent chloride diffusion coefficients by slag-blended concrete. Fan and Wang [11] presented a numerical model to analyse cement hydration reaction and chloride ion penetration process simultaneously. In the study of Han [12], modified

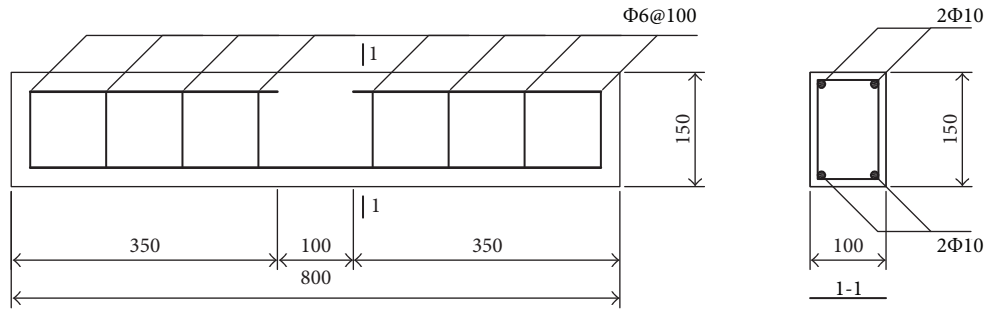

Figure 1: Geometry size and reinforcement of beam specimens.

chloride diffusion coefficient was proposed as a function of chloride binding, evaporable water content, and diffusion coefficient. In coastal environments, alternation of dry and wet accelerates the transmission of chloride into concrete. Chloride ingress under wet-dry cycles was conducted by many researches. In the study of Li et al. [13], under dry-wet cycles influential depth of moisture transport in concrete was analysed to obtain water loss and intake balance, based on which an equilibrium drying-wetting time ratio was proposed. In the study of Wu et al. [14], the influences of dry-wet cycles, stress ratios, and exposed ages on chloride ions transport in concrete were studied and the chloride diffusion coefficient under loads was calculated by regression method. In the study of Ye et al. [15, 16], to describe the transport of chloride ions in cracked concrete under dry-wet cycles, crack width, crack surface roughness, tortuosity, and capillary pores at crack surface were considered to develop a model by Poiseuille law.

In coastal environment, both chloride diffusivity and mechanical performance need to be considered to study the durability of RC structures. Diao et al. [17] experimentally studied the durability and bearing capacity of RC beams under combined action of environmental and sustained loading. The effect of air content (3.2% and 6.1%) was considered. The results showed that the yield load, as well as the ultimate load, and the ductility of RC beams with higher air content increased after the combined action of freeze-thaw cycles and seawater immersion. Shen et al. [18] studied the effect of sea water wet-dry cycle on mechanical performance of eccentric RC columns with different crack width and found that the bearing capacity decreased obviously when the crack width exceeded 0.1 mm.

However, the studies considering initial damage from cyclic loading were fewer in the existing literature. In coastal environment, the RC bridges structures are under combined action of cyclic loading and seawater wet-dry cycle. This paper reports on laboratory experiments on RC beam specimens after combined effects of cyclic load and seawater wet-dry cycles, which included two steps. First, to simulate initial damage, cyclic loading was controlled by max load and cycles. During every cycle, max load was 0.4, 0.5, and 0.6 times ultimate load. And 1, 5, 10, and 20 cycles of loading were applied on RC beam specimen. Second, coastal chloride environment was simulated in laboratory by 240 alternate action of seawater wet and dry. After 240 times seawater wet-dry cycles, chloride diffusivity and mechanical performance of RC beam specimen were tested and analysed.

Table 1: The proportions of concrete mixture.

Concrete composition (/m^3)	(/kg)
Cement	500
Water	225
River sand	660
Coarse aggregate	990
Fly ash	60
Water reducer	8 L

2. Experimental Method

2.1. RC Beam Specimens. Fourteen RC beam specimens were designed with same size, reinforcements, and concrete. As shown in Figure 1, the beam specimen size was 100 mm × 150 mm × 800 mm and the concrete cover was 35 mm. Deformed steel bars with diameter 10 mm were used as tensile bars and plain steel bars with diameter 6 mm were used as stirrups. The yield strength and ultimate strength of the tensile bar were 349 MPa and 456 MPa, respectively. Concrete was made of ordinary Portland cement, gravel, river sand, fly ash, and water reducer. The maximum size of coarse aggregate was 10 mm. The proportion of concrete mixture was shown in Table 1. 28 d concrete cubic compressive strength was 55 MPa.

2.2. Experimental Method

2.2.1. Loading History. This paper focuses on initial damage from cyclic loading. The bending load increased from 0 to max load and decreased to 0, which formed one cycle of loading. Different cycles of loading were applied to beam specimen to simulate cyclic loading. Table 2 gives test condition of beam specimens. In Table 2, P_u was ultimate load of beam specimen B-Ref at the age of 28 d and the value of P_u was 40.5 kN. P_u was reference to max load of all beam specimen. To explain loading history, beam specimen B-0.6P20C was taken as an example. During every cycle of loading, the bending load increased from 0 to $0.6P_u$ and

Table 2: Test condition of beam specimens.

Specimen	Cyclic loading		Environment
	Max load	Cycles	
B-0P0C	$0.0P_u$	0	W-D cycle
B-0.4P1C	$0.4P_u$	1	W-D cycle
B-0.5P1C	$0.5P_u$	1	W-D cycle
B-0.6P1C	$0.6P_u$	1	W-D cycle
B-0.4P5C	$0.4P_u$	5	W-D cycle
B-0.5P5C	$0.5P_u$	5	W-D cycle
B-0.6P5C	$0.6P_u$	5	W-D cycle
B-0.4P10C	$0.4P_u$	10	W-D cycle
B-0.5P10C	$0.5P_u$	10	W-D cycle
B-0.6P10C	$0.6P_u$	10	W-D cycle
B-0.4P20C	$0.4P_u$	20	W-D cycle
B-0.5P20C	$0.5P_u$	20	W-D cycle
B-0.6P20C	$0.6P_u$	20	W-D cycle
B-Ref	0	0	No

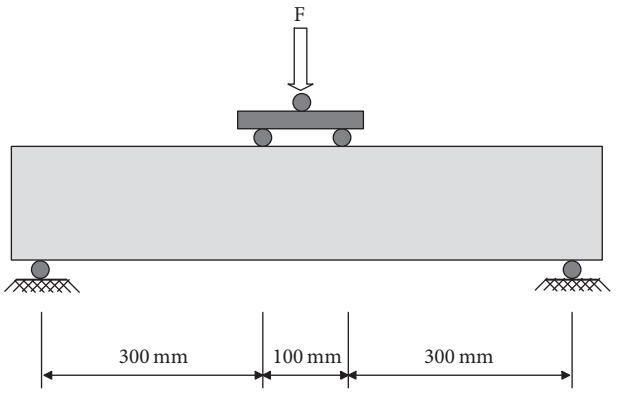

Figure 2: Schematic diagram of 4-point bending on beam specimens.

decreased to 0.20 cycles of loading was applied to beam specimen B-0.6P20C. Figure 2 gives the diagram of loading test. As shown in Figure 2, 4-point bending test was adopted for all beam specimens. After cyclic loading, the crack widths on beam specimens were measured and measuring points were marked to track the evolution of crack width during seawater corrosion.

2.2.2. Simulation of Seawater Corrosion. The w-d cycle was alternative action of seawater spraying and air drying (atmosphere environment). Every w-d cycle lasted 6 h, including 5 h air drying and 1 h seawater spraying, that is, wet : dry time = 1 : 5. To apply wet-dry cycle in laboratory, a self-designed automatic sprinkler system was used. Figure 3 exhibits the schematic diagram of the automatic sprinkler system for w-d cycle. The simulated sea water (hereinafter referred to as seawater) was artificially made of 3.5% NaCl (mass fraction). All beam specimens experienced 240 w-d cycles.

2.2.3. Mechanical Performance and Chloride Content Test. After 240 w-d cycles of seawater, mechanical performance

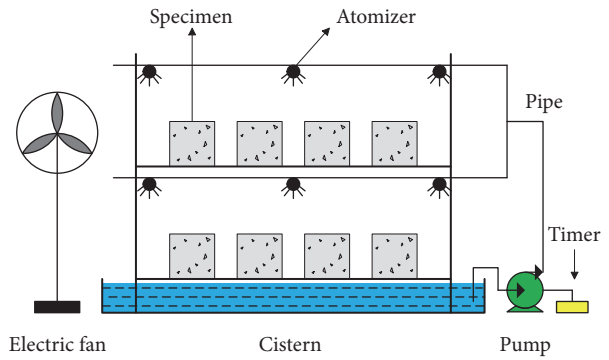

Figure 3: Schematic diagram of the automatic sprinkler system for seawater w-d cycle.

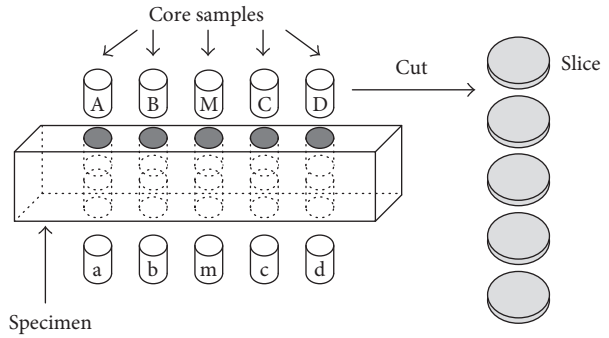

Figure 4: Schematic diagram of core sample drilling and sheet subcutting.

of beam specimen was tested. The 4-point bending test was conducted on beam specimens to study the residual yield load, ultimate load, and ductility. After the failure of beam specimen, chloride content was tested. Figure 4 gives the schematic diagram of core sample drilling and sheet subcutting. As shown in Figure 4, core samples with diameter of 50 mm were drilled in the tension of concrete (positions a, b, m, c, d) and the compression concrete (positions A, B, M, C, D). The spacing of drilling position was 100 mm. The core sample was then cut into 5 pieces of slices and then the slices were grinded up to powder. According to the test results, the free chloride content (percentage of cementitious material) in different positions and depths of concrete can be obtained by Ion Selective Method [19].

3. Testing Results and Discussion

3.1. Evolution of Crack Width. During cyclic loading, cracks appeared in tension concrete of beam specimen. The crack width in same position was monitored before and after w-d cycle. On account of various crack developing, 3 measuring points were demanded at least for each crack; therefore dozens of measuring points were set and marked for tracking every crack. The variation of crack width before and after w-d cycle was collected in Table 7. Both width and number of cracks increased as max load and cycle increased. The

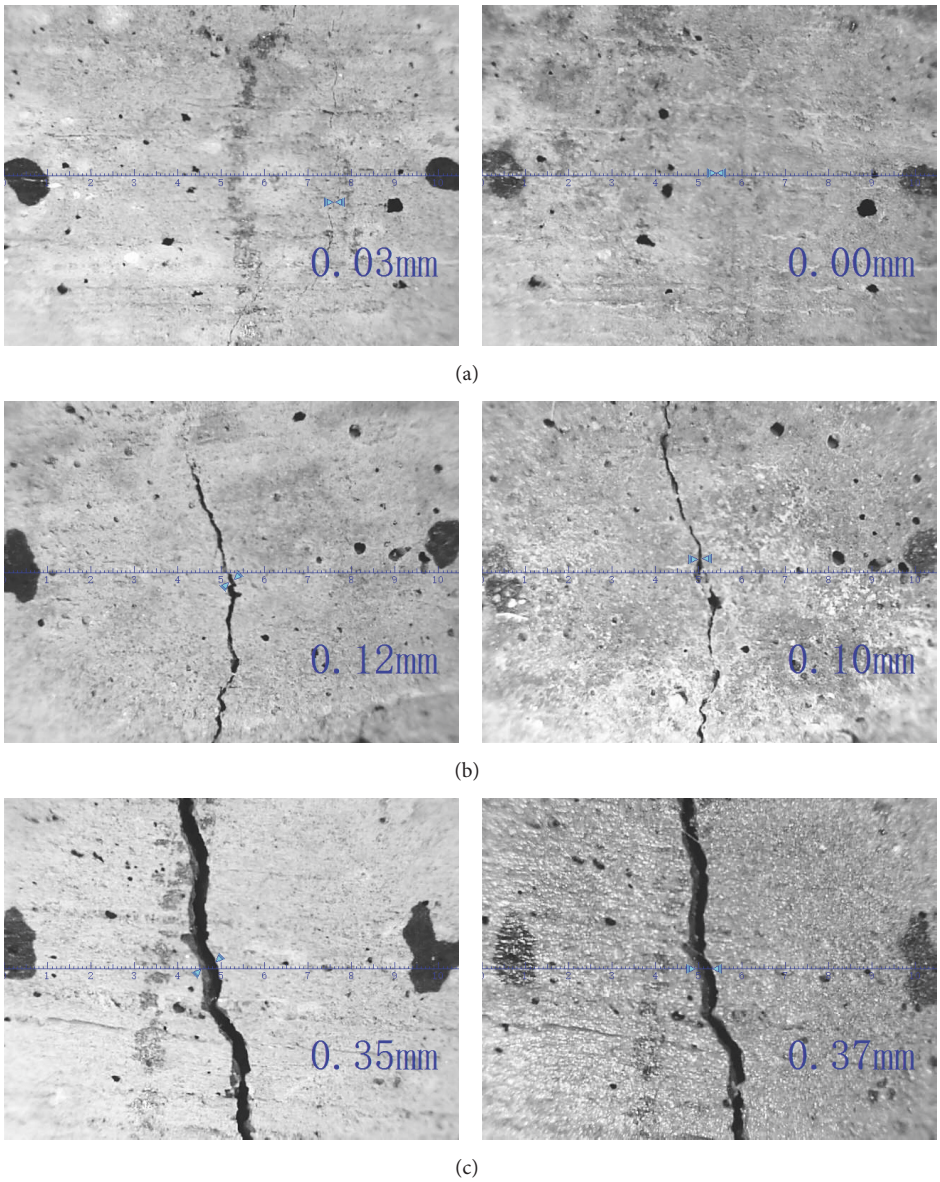

Figure 5: Evolution of crack width before (left) and after (right) w-d cycles: (a) completely self-healing; (b) partly self-healing; (c) remaining stable.

maximum crack width of specimens B-0.4P1C, B-0.4P5C, and B-0.4P10C was below 0.2 mm when the cyclic loading was $0.4P_u$. When max load was higher the cracks became wider and the maximum crack width exceeded 0.2 mm. During the period of w-d cycle, self-healing completely was observed when crack width was narrower than 0.1 mm and self-healing partly was observed when crack width ranged from 0.1 to 0.2 mm. When crack width was wider than 0.2 mm, the cracks remained relatively stable after w-d cycles. When the cracks width was narrower than 0.1 mm, self-healing was observed. Due to the hydration reaction in cracks, the production of reaction $CaCO_3$ is insoluble in water and subsequently filled the cracks, which can be verified with XPS [2]. Figure 5 shows three typical situations of the crack width before and after w-d cycles.

3.2. The Chloride Ion Transmission in Concrete

3.2.1. Chloride Transmission Model in W-D Cycle Environment. The chloride ion penetrates into concrete mainly by diffusion and convection under w-d cycles. (1) Diffusion: the chloride ion moves from high to low concentration in the pore solution due to the concentration gradient. (2) Convection: when the liquid permeates in porous medium, the solute is transported with the liquid from high pressure to low pressure due to the pressure gradient. The two types of chloride ion transfer pattern exist at the same time. When the concrete turned from drying to wetting in the w-d cycles, the seawater transferred rapidly into the dry concrete carrying a great deal of chloride ion. The transfer effect of chloride ion convection is stronger than diffusion

in the near surface region because the saturation gradient is great near the concrete surface. In the inner concrete, the variation of saturation with depth is small and chloride ion transferred mainly by diffusion. In w-d cycle, the liquid loss and intake affect a limited depth from concrete surface [13, 20]. When the liquid permeates in concrete, the chloride ion is transported with the liquid and hence generates the convection flux:

$$j_{c,\mathrm{cl}} = q_w \cdot c, \tag{1}$$

$$q_w = \frac{j_w}{\rho_l}. \tag{2}$$

c is chloride ion content (mol/m^3). q_w is liquid volumetric flux (m/s) and can be expressed by $j_w \cdot \rho_l$ is liquid density. The chloride ion diffusion flux can be calculated by

$$j_{d,\mathrm{cl}} = -D_{\mathrm{cl}} \nabla c. \tag{3}$$

D_{cl} is diffusion coefficient of chloride ion Θ which is saturation of concrete.

The total chloride ion flux in concrete is

$$j_c = j_{c,\mathrm{cl}} + j_{d,\mathrm{cl}}. \tag{4}$$

The chloride ion mass conservation can be expressed as

$$\frac{\partial c}{\partial t} = -\nabla \cdot j_{\mathrm{cl}}. \tag{5}$$

From (1), (3), (4), and (5), the chloride ion transfer equation can be expressed as

$$\frac{\partial c}{\partial t} = \nabla \left[D_{\mathrm{cl}} \nabla c \right] - \nabla \left(q_w c \right). \tag{6}$$

In (6), the chloride ion absorption is ignored. Due to the fact that influence region of w-d cycles on chloride ion transfers to the near surface of concrete, the chloride ion transfer equation can be expressed as (7) in deeper concrete which is affected by diffusion.

$$\frac{\partial c}{\partial t} = \nabla \left[D_{\mathrm{cl}} \nabla c \right]. \tag{7}$$

The concrete was in nonsaturation state during w-d cycle and therefore D_{cl} is a function of saturation Θ and diffusion time t. Due to the fact that chloride ion only can diffuse in pore solution, there are two reasons causing D_{cl} decrease when Θ decreased: (1) the area used for transmission is reduced; (2) the transmission path for chloride ion becomes longer because part of the pore is not connected. The influence of Θ has been investigated by several researchers [21–24]. The chloride ion diffusion coefficient decreased as concrete age increased because of the continuous hydration of the binders. In Tang and Nilsson's research [25] and Life-365 program [26], (8) was used which contained the effect of time.

$$D_{\mathrm{cl}}(t) = D_{\mathrm{ref}} \left(\frac{t_{\mathrm{ref}}}{t} \right)^m, \tag{8}$$

where D_{ref} is the chloride ion diffusion coefficient at time t_{ref} = 28 days and m is the diffusion decay factor. In this study, core samples with diameter of 50 mm were drilled in the cover of beam specimen. The chloride ion transferred into concrete from two directions: (1) the top (or bottom) surface and (2) the side surface of concrete beam. Therefore, the chloride ion of core sample consisted of two-direction ingress. The chloride content from side direction ingress was only from the region whose depth was 25 mm to 75 mm (started from side surface) because the drill hole was in the centre of top (or bottom) surface of concrete beam. However, the chloride ion content change rate is rather small when the depth of concrete was greater than 25 mm. Hence, the chloride ingress from side direction had an ignorable influence on chloride ingress from top (or bottom) direction in the region of core sample. Assuming chloride ion transmission into concrete in core sample region to be one dimensional, (7) can be expressed as (9) when taking concrete saturation and ageing effect into account:

$$\frac{\partial c}{\partial t} = \left(\frac{t_{\mathrm{ref}}}{t} \right)^m \cdot \left[\frac{\partial D_{\mathrm{cl,ref}}(\Theta)}{\partial \Theta} \cdot \frac{\partial \Theta}{\partial x} \cdot \frac{\partial c}{\partial x} + D_{\mathrm{cl,ref}}(\Theta) \cdot \frac{\partial^2 c}{\partial x^2} \right], \tag{9}$$

where $D_{\mathrm{cl,ref}}(\Theta)$ is the chloride ion diffusion coefficient when $t = t_{\mathrm{ref}}$. In this study, the w-d cycle was wetting dominated and the saturation of deeper concrete remained stable with time and depth. For this reason, $D_{\mathrm{cl,ref}}(\Theta) = D_{\mathrm{cl,ref,non}}$ is a constant where $D_{\mathrm{cl,ref,non}}$ is the chloride ion diffusion coefficient when $t = t_{\mathrm{ref}}$ and saturation $\Theta \neq 100\%$. Hence, (9) changes to (10):

$$\frac{\partial c}{\partial t} = D_{\mathrm{cl,ref,non}} \cdot \left(\frac{t_{\mathrm{ref}}}{t} \right)^m \cdot \frac{\partial^2 c}{\partial x^2}. \tag{10}$$

Equation (10) is a nonlinear partial differential equation. To solve (10), variable substitution is used as follows where t_0 is the age of concrete when chloride ion ingress begins:

$$T = \int_{t_0}^{t} D_{\mathrm{cl,ref,non}} \cdot \left(\frac{t_{\mathrm{ref}}}{t} \right)^m dt = \begin{cases} \dfrac{D_{\mathrm{cl,ref,non}} \cdot t_0^m}{1-m} \left(t^{1-m} - t_0^{1-m} \right) & m \neq 1 \\ D_{\mathrm{cl,ref,non}} \cdot t_0 \ln \dfrac{t}{t_0} & m = 1, \end{cases} \tag{11}$$

$$\frac{dT}{dt} = D_{\mathrm{cl,ref,non}} \cdot \left(\frac{t_{\mathrm{ref}}}{t} \right)^m.$$

According to the derivation rule of compound function,

$$\frac{\partial c}{\partial t} = \frac{\partial c}{\partial T} \cdot \frac{dT}{dt} = D_{\mathrm{cl,ref,non}} \cdot \left(\frac{t_{\mathrm{ref}}}{t} \right)^m \cdot \frac{\partial c}{\partial T}. \tag{12}$$

Equation (13) can be obtained by comparing (10) and (12):

$$\frac{\partial c}{\partial T} = \frac{\partial^2 c}{\partial x^2}. \tag{13}$$

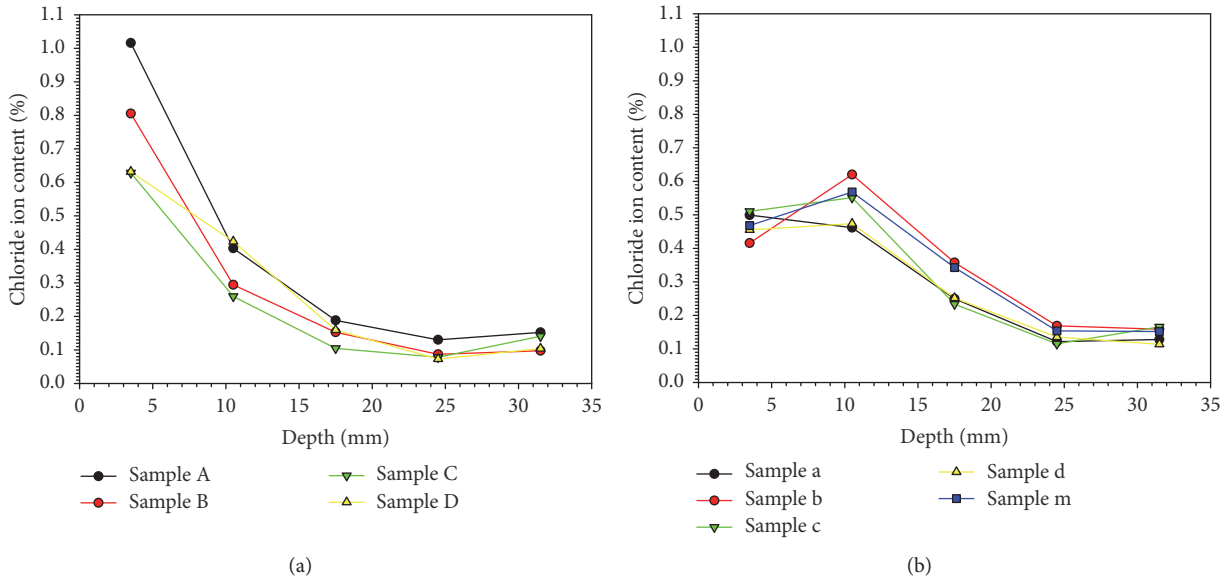

Figure 6: Chloride profiles of beam specimen B-0.4P5C. (a) Compression concrete. (b) Tension concrete.

Considering three boundary conditions, (1) the content of chloride ion on concrete surface is constant, $C(x = 0, t) = C_s$; (2) the content of chloride ion in concrete is C_0 at the initial time, $C(x, t = 0) = C_0$; (3) the content of chloride ion in concrete is C_0 at infinity, $C(x = \infty, t) = C_0$, a special solution can be obtained from (13).

$$C(x,T) = C_0 + (C_s - C_0)\left[1 - \operatorname{erf}\left(\frac{x}{2\sqrt{T}}\right)\right] C(x,t)$$

$$= \begin{cases} C_0 + (C_s - C_0)\left[1 - \operatorname{erf}\left(\dfrac{x}{\sqrt{4D_{\mathrm{cl,ref,non}} \cdot t_0^m \left(t^{1-m} - t_0^{1-m}\right) / |1-m|}}\right)\right] & m \neq 1 \\ C_0 + (C_s - C_0)\left[1 - \operatorname{erf}\left(\dfrac{x}{\sqrt{4D_{\mathrm{cl,ref,non}} \cdot t_0 \left|\ln t/t_0\right|}}\right)\right] & m = 1. \end{cases} \tag{14}$$

3.2.2. Test Results of Chloride Content and Analysis of Chloride Ion Diffusivity. Figure 6 shows the chloride profiles of beam specimen B-0.4P5C. Because the chloride profiles from all beam specimens were similar, hence the chloride profiles of beam specimen B-0.4P5C were taken as example to illustrate the chloride ion distribution. As can be seen from Figure 6, the chloride content of tension concrete was higher than that in compression concrete and the chloride content decreased as depth increased.

The relationship between chloride content at steel surface (depth 31.5 mm) and average crack width (ω_{avg}) is shown in Figure 7. As shown in Figure 7, the chloride content increased approximatively linearly as average crack width increased. This implied that the effect of chloride ion transmission became more obvious when crack width increased.

Figure 8 shows chloride content at steel surface and sum of chloride ion content in concrete cover with max load and cycle. As shown in Figure 8, the chloride content increased as max load increased. Compared with other specimens, chloride content was most when beam specimens experienced 20 cycles of loading. It can be concluded that the chloride content at steel surface was affected by max load. The higher max load led to wider cracks and hence more chloride ion transferred into concrete. What is more, compared with the effect of max load, the effect of cycle on chloride content was little. A possible explanation was that, under the same max load, the crack width differed insignificantly when cycles increased from 1 to 10. The influence of cyclic load on crack width was discernible when cycles were 20. As can be observed from Figure 8(a), for the specimens whose average crack width was below 0.10 mm (under the lower line in Figure 8), the difference of chloride content was minor. For the specimens whose average crack width exceeded 0.13 mm (above the higher line in Figure 8), the chloride content increased obviously. As shown in Figure 8(b), the sum of chloride content in tension concrete increased as the max

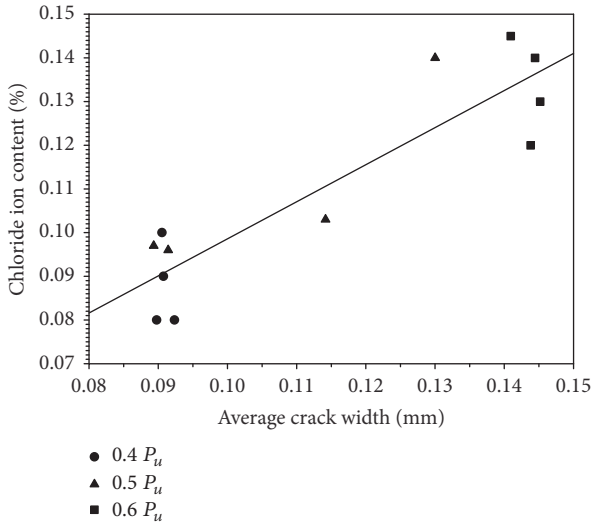

Figure 7: Relationship between chloride content at steel surface and average crack width.

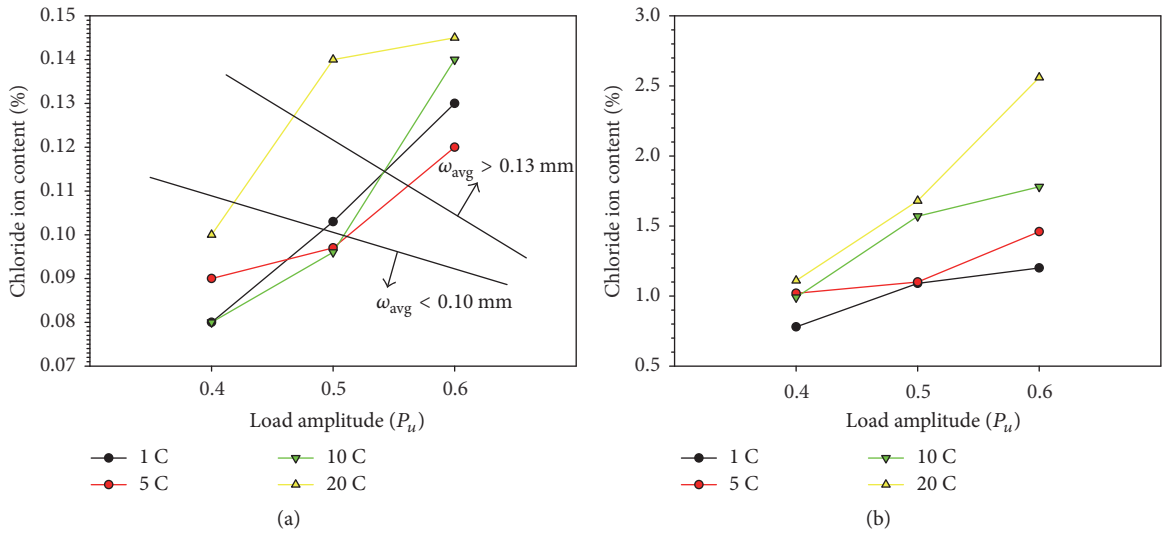

Figure 8: (a) Chloride ion content with load amplitudes and cycle numbers at steel depth. (b) Accumulation chloride ion content in tensile concrete cover.

load amplitude and cycle increased. The sum of chloride content intension concrete mainly depended on the crack width which was controlled by max load.

In this study, the values of different parameters are t_0 = 80 days, t_0 = 140 days, and m = 0.28 following the research of Park et al. [10] and the Chinese standard for durability assessment of concrete structures [27], C_0 = 0.0008 mol/L. There are two unknown parameters C_s and $D_{cl,ref,non}$ remaining in (14). The unknown parameters can be estimated by using nonlinear least-squares fitting method in MATLAB. Equation (14) is used to fit the results of chloride content in concrete. The data of chloride content in deeper concrete was used in fitting. The residual sum of squares of fitting function is below 1×10^{-4}. A part of fitting curves are shown in Figure 9 as an example.

In order to evaluate the average chloride ion diffusion effect during chloride ingress, the average chloride ion diffusion coefficient D_{avg} is calculated as follows:

$$D_{avg} = \frac{\int_{t_0}^{t} D_{cl,ref,non} \left(t_{ref}/t\right)^m dt}{t - t_0}. \quad (15)$$

Figure 10 shows the value of D_{avg} in different core sample position. Specimens B-0.4P20C and B-0.5P5C were taken as example. The missing value of position M in compression side was due to the concrete crush. The difference of D_{avg} between tension concrete and compression concrete was not significant in the uncracked position such as sample a, d in Figure 10. D_{avg} in sampling position which contained cracks or near cracks was higher than the other positions. It indicates

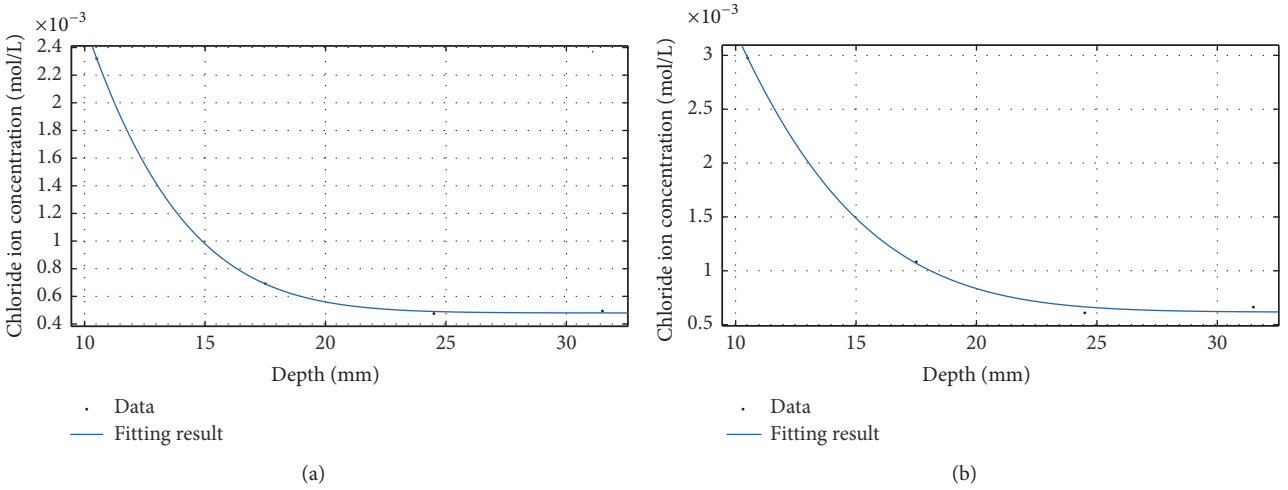

Figure 9: Curve fitting of chloride ion concentration.

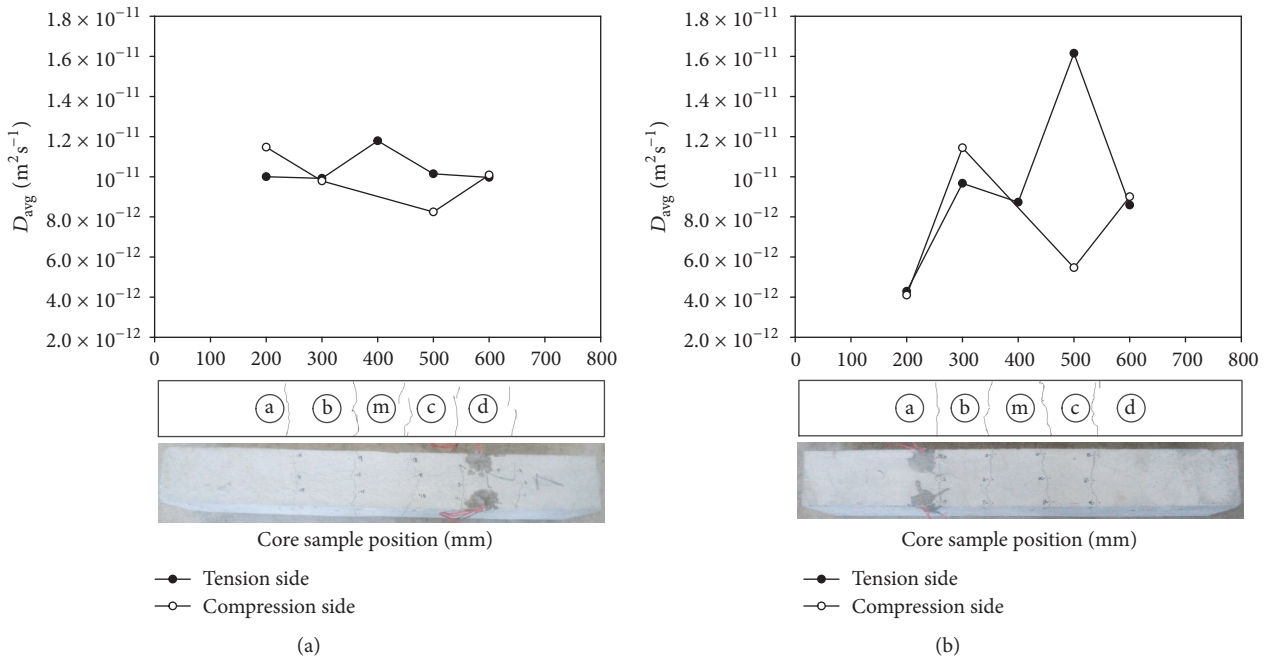

Figure 10: Average chloride diffusion coefficient in different core sample position.

that the value of D_{avg} was significantly affected by crack distribution.

D_{avg} values of core samples with cracks are exhibited in Figure 11. The mean of D_{avg} in uncracked concrete was calculated from the uncracked core samples and showed in Figure 11 as a long dash line. As can be observed, D_{avg} increased as crack width increased when the crack width was less than 0.11 mm whereas the increasing tendency was weak when the crack width exceeded 0.11 mm. Moreover, when the crack width increased from 0.11 mm to 0.23 mm, D_{avg} ranged from 1.1 to 1.6×10^{-11} m^2/s which were 1.9 to 2.4 times D_{avg} of uncracked concrete. This was similar to the study of Djerbi et al. [28]. It was concluded that the influence of crack width on D_{avg} may not be linear and cracks can enhance the effect of chloride penetration.

3.3. Results of Loading Test. For all of the beam specimens, the failure mode was bending failure, where tensile reinforcement bars yielded and then concrete in the compression zone crushed. Table 3 gives the testing results of 4-point monotonic loading of beam specimens which were damaged by cyclic loading and suffered 240 w-d cycles of seawater. As shown in Table 3, for the same cycles, the residual yielding load and ultimate load decreased as max load increased. And for the same max load, the residual yielding load and ultimate load decreased as cycles increased. These results indicated that the

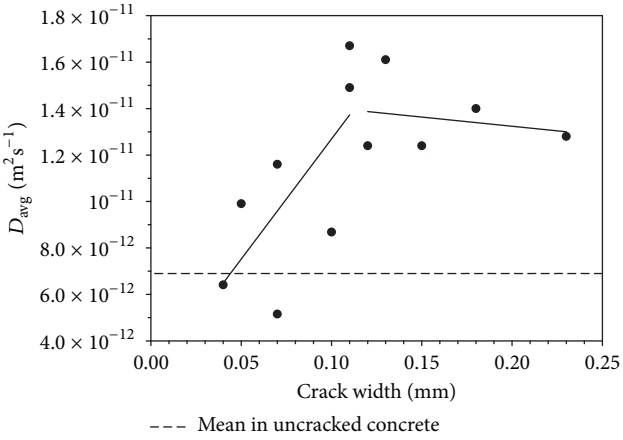

Figure 11: Average chloride diffusion coefficient in crack region. Black circles refer to average chloride diffusion coefficients. Solid lines refer to linear regression.

Table 3: Testing results of beam specimens under monotonic loading.

Specimen	Yield load		Ultimate load		Ultimate deflection	Ductility
	P_y/kN	δ_y/mm	P_u/kN	δ_u/mm	δ_f/mm	δ_f/δ_y
B-0P0C	41.09	2.06	50.50	17.37	37.82	18.4
B-0.4P1C	36.81	2.75	46.51	31.23	36.25	13.2
B-0.4P5C	36.20	3.21	41.28	15.51	16.34	5.09
B-0.4P10C	36.12	3.01	42.96	16.84	28.89	9.60
B-0.4P20C	30.08	3.44	39.66	18.79	19.81	5.76
B-0.5P1C	33.03	2.56	41.99	20.56	26.89	10.5
B-0.5P5C	31.29	3.66	34.98	20.31	22.16	6.05
B-0.5P10C	32.11	2.93	36.56	10.41	18.01	6.15
B-0.5P20C	29.29	4.38	35.76	15.03	18.55	4.24
B-0.6P1C	27.32	2.27	38.79	17.54	17.81	7.8
B-0.6P5C	28.50	3.40	36.69	16.50	28.16	8.28
B-0.6P10C	28.42	3.01	35.46	17.59	24.95	8.29
B-0.6P20C	23.09	3.41	34.05	18.25	22.62	6.63

Note. P_y is yield load, δ_y is the span center deflection corresponding to yield load, P_u is the ultimate load and corresponding deflection δ_u at the midspan, δ_f is the ultimate deflection which corresponds to the load when decreasing to 85% of ultimate load, and δ_f/δ_y is displacement ductility factor.

load amplitude, cycle number, and w-d cycles of seawater influenced obviously the residual mechanical performance of RC beams.

The load-deflection curves of beam specimens were shown in Figure 12. As listed in Table 3 and shown in Figure 12, after damage by cyclic loading and 240 w-d cycles of seawater, the residual yield load and ultimate load decreased rapidly as max load increased. Compared with undamaged RC beam specimens, the ductility of RC beams damaged by cyclic loading reduced significantly. It was concluded that the combined action of cyclic load and seawater w-d cyclic had a great impact on mechanical performance of beam specimens.

3.4. Degradation of Mechanical Performance. Compared with the beam specimen B-0P0C, which was in the same environment but undamaged by cyclic loading, the reduction of yield load, ultimate load and ductility of other beams are shown in Table 4. Figure 13 exhibits the yield load and ultimate of beam specimen subjected to different max load. As shown in Table 4 and Figure 13, after being damaged by cyclic load and experienced 240 w-d cycles of seawater, the residual yield load and ultimate load of beam specimens reduced as max load and cycles increased.

Difference of yield load and ultimate reduction between 1 cycle, 5 cycles, and 10 cycles was insignificant. Compared with beam specimen after 1 cycle of loading, the reduction of yield load and ultimate load was analysed. After 20 cycles of loading whose max load was $0.4P_u$, the yield load decreased by 18.3% and the ultimate load decreased by 14.7%. After 20 cycles of loading whose max load was $0.6P_u$, the yield load decreased by 15.5% and the ultimate load decreased by 12.2%. It implied that, under the same max load, cycle times have greater impact on the yield load than on the ultimate load. When cycles were 20, the yield load and ultimate load decreased obviously under the same max load. This shows that the cycle had a great influence on the

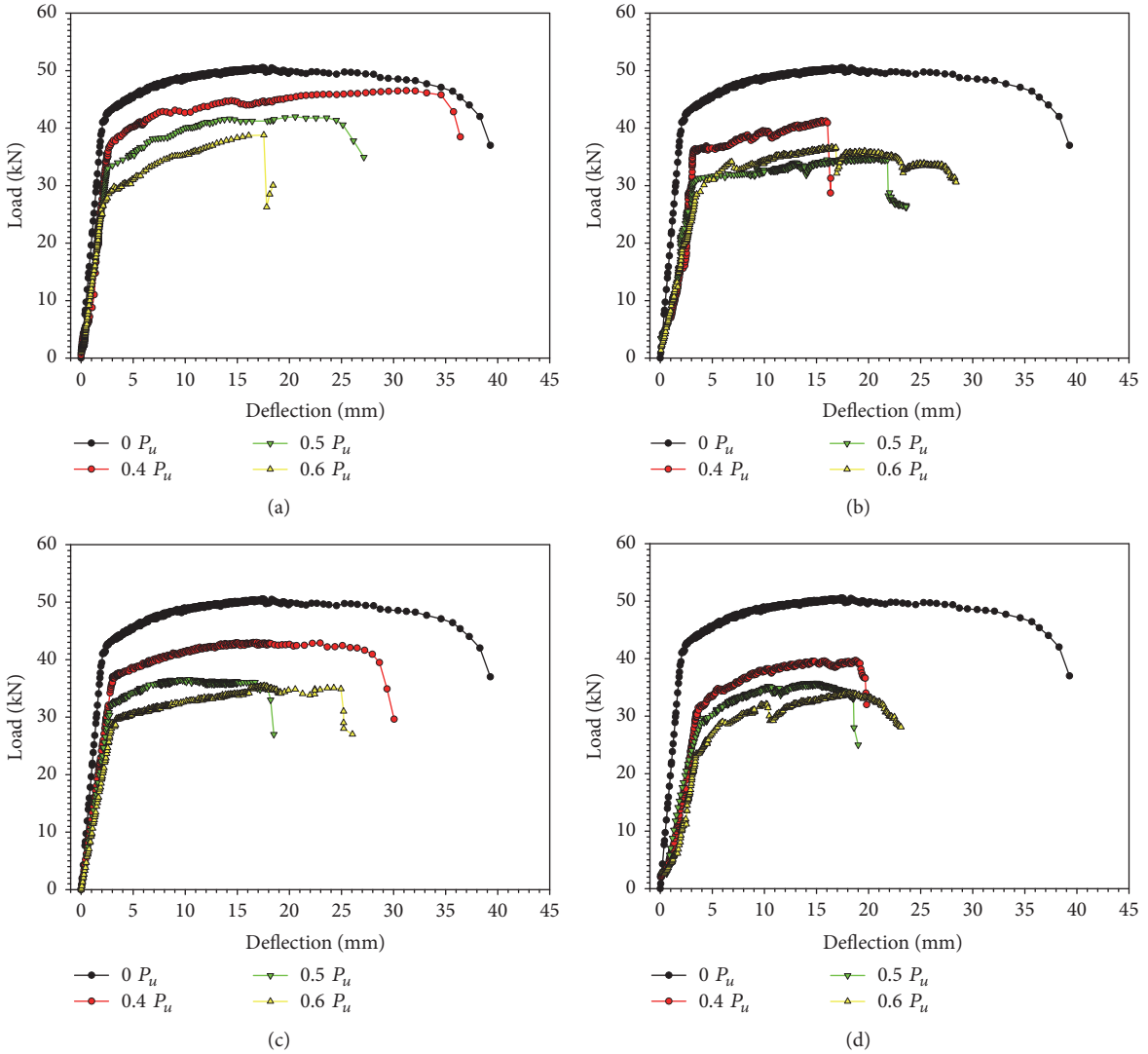

Figure 12: Load-deflection curves of RC beams: (a) 1 cycle; (b) 5 cycles; (c) 10 cycles; (d) 20 cycles.

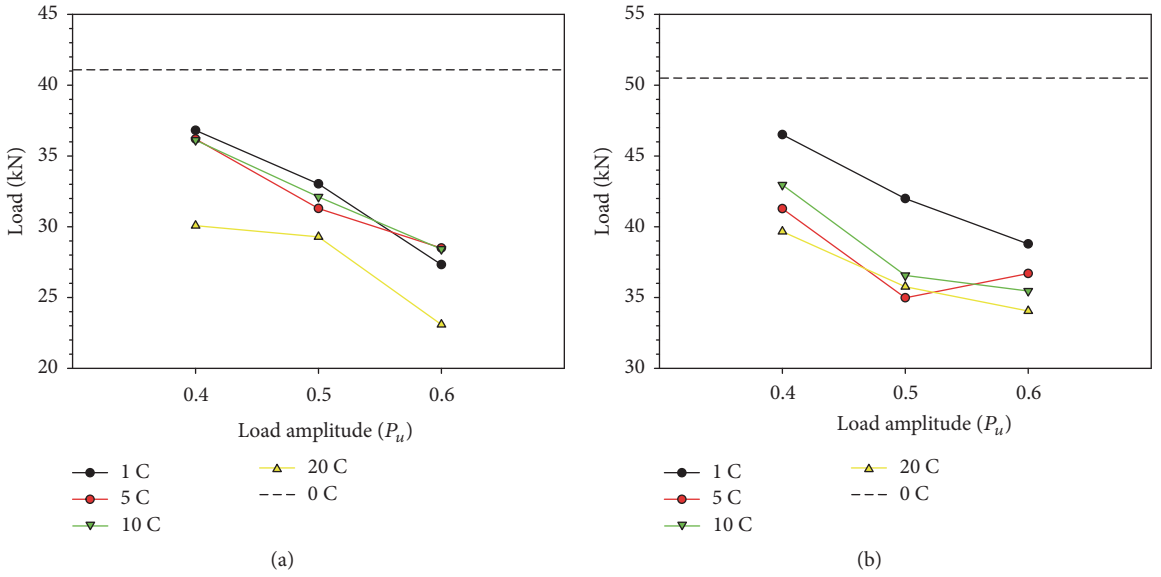

Figure 13: Yield load and ultimate load with load amplitudes and cycle numbers: (a) yield load; (b) ultimate load.

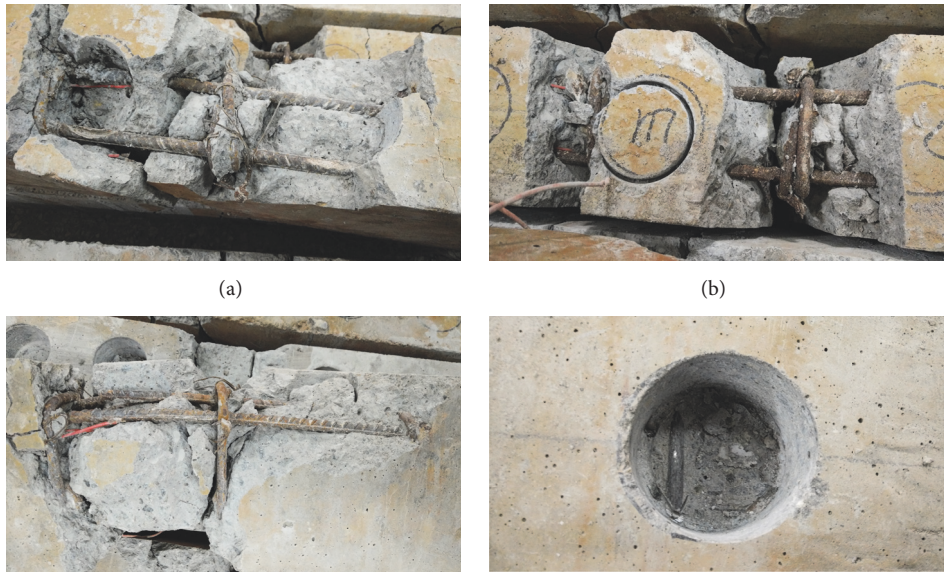

(a) (b) (c) (d)

Figure 14: Corrosion of steel reinforcement in concrete ((a), (b), (c)) crack region and (d) uncracked region.

Table 4: Reduction of yield load, ultimate load, and ductility of specimens.

Specimen	Reduction		
	ΔP_y/%	ΔP_u/%	$\Delta\mu^a$/%
B-0.4P1C	10.4	7.9	28.3
B-0.4P5C	11.9	18.3	72.3
B-0.4P10C	12.1	14.9	47.8
B-0.4P20C	26.8	21.5	68.7
B-0.5P1C	19.6	16.9	42.9
B-0.5P5C	23.9	30.7	67.1
B-0.5P10C	21.9	27.6	66.6
B-0.5P20C	28.7	29.2	77.0
B-0.6P1C	33.5	23.2	57.6
B-0.6P5C	30.6	27.3	55.0
B-0.6P10C	30.8	29.8	54.9
B-0.6P20C	43.8	32.6	64.0

Note. [a]Displacement ductility factor.

degradation of mechanism performance of RC beams. From Table 7, the maximum crack width of specimen B-0.4P1 was less than 0.2 mm; however the reduction of yield load and ultimate load exceeded 5% and the reduction of ductility ratio exceeded 20%. Under combined action of cyclic loading and w-d cycles of seawater, the reduction of yield load and ultimate load of beam specimen after 5, 10, and 20 cycles of loading were more than 12%, even though the max load was $0.4P_u$.

After beam specimens were damaged by cyclic load and experienced 240 w-d cycles of seawater, the corrosion of steel reinforcement in cracked region was found due to chloride ingress, as shown in Figures 14(a), 14(b), and 14(c). However, visually corrosion of steel bars was not found in uncracked region by drilling several holes as Figure 14(d). As shown in Figures 14(a), 14(b), and 14(c), the most serious corrosion occurred in crack position and corrosion was observed to be gradually weakened along steel bar from crack position to uncracked concrete. This could be responsible for the degradation of mechanical performance of beam specimens.

A univariate analysis of variance was conducted with SPSS statistical software. The dependent variable was reduction of yield load and ultimate load and factors were cycle and max load. The results are shown in Table 5. From Table 5(a), the significance levels of cycle and max load are below 0.05, which means that cycle and max load had a significant impact on reduction of yield load and ultimate load. Besides, max load had a more pronounced effect on reduction of yield load and ultimate load than cycle. The crack width increased obviously as max load increased. However, it increased gently as the cycle increased under the same max load. It implied that max load played a main role in the reduction of yield load and ultimate load. Tables 5(b) and 5(c) show the results of multiple comparisons. As shown in Table 5(b), the cycle can be divided into two subsets. One subset includes 1, 5, and 10 and the other includes 20, which means that the effect of cycle number on yield load reduction increased when cycle was 20. The differences were not statistically significance between different max loads by making multiple comparisons. When the dependent variable changed to reduction of ultimate load, the groups whose cycle was 1 and max load was $0.4P_u$ had a significant difference compared with other groups but the other intergroup differences were not statistically significance.

Table 6 shows the comparison of bending rigidity of beam specimens between before and after w-d cycles. As shown in Table 6, the bending rigidity of specimens decreased and

Table 5

(a) Tests of between-subjects effects

Dependent variable	Source	Type III sum of squares	Df	Mean square	F	Sig.
Reduction of yield load	Corrected model	1053.732[a]	5	210.746	30.072	0.000
	Intercept	7203.000	1	7203.000	1027.817	0.000
	Cycles	**297.247**	**3**	**99.082**	**14.138**	**0.004**
	Max load	**756.485**	**2**	**378.242**	**53.973**	**0.000**
	Error	42.048	6	7.008		
	Total	8298.780	12			
	Corrected total	1095.780	11			
Reduction of ultimate load	Corrected model	597.754[b]	5	119.551	22.438	0.001
	Intercept	6528.667	1	6528.667	1225.338	0.000
	Cycles	**235.289**	**3**	**78.430**	**14.720**	**0.004**
	Max load	**362.465**	**2**	**181.233**	**34.015**	**0.001**
	Error	31.968	6	5.328		
	Total	7158.390	12			
	Corrected total	629.723	11			

Note. [a]R squared = 0.962 (adjusted R squared = 0.930). [b]R squared = 0.949 (adjusted R squared = 0.907).

(b) Post hoc test (dependent variable: reduction of yield load)

Cycles	N	Subset		Max load	N	Subset		
		1	2			1	2	3
1	3	21.1667		$0.4P_u$	4	15.3000		
10	3	21.6000		$0.5P_u$	4		23.5250	
5	3	22.1333		$0.6P_u$	4			34.6750
20	3		33.1000					
Sig.		0.680	1.000	Sig.		1.000	1.000	1.000

Note. The error term is mean square (error) = 7.008. Alpha = 0.05.

(c) Post hoc test (dependent variable: reduction of ultimate load)

Cycles	N	Subset		Max load	N	Subset	
		1	2			1	2
1	3	16.0000		$0.4P_u$	4	15.6500	
10	3		24.1000	$0.5P_u$	4		26.1000
5	3		25.4333	$0.6P_u$	4		28.2250
20	3		27.7667				
Sig.		1.000	0.109	Sig.		1.000	0.241

Note. The error term is mean square (error) = 5.328. Alpha = 0.05.

Table 6: Comparison of bending rigidity of specimens between before and after w-d cycles.

Specimen	Before w-d cycles B/kN·m^2	After w-d cycles B/kN·m^2	Reduction ΔB/%
B-0P0C	—	41.03	—
B-0.4P1C	33.82	32.14	4.9
B-0.4P5C	23.85	22.59	5.3
B-0.4P10C	30.33	24.62	18.8
B-0.4P20C	20.76	16.4	21.0
B-0.5P1C	27.43	25.18	8.2
B-0.5P5C	28.79	26.60	7.6
B-0.5P10C	28.27	22.95	18.8
B-0.5P20C	26.87	20.64	23.2
B-0.6P1C	28.88	24.36	15.7
B-0.6P5C	23.87	20.72	13.2
B-0.6P10C	29.46	20.47	30.5
B-0.6P20C	25.33	17.91	29.3

the degree of reduction increased as max load increased. The bending rigidity of beam specimens after 20 cycles of loading deceased obviously compared with beam specimens after 1 cycle.

4. Conclusions

An experimental study was conducted to investigate the impact of cyclic loading on the mechanical performance and chloride diffusivity of RC beams exposed to seawater wet-dry cycles. Based on the results of monotonic loading and analysis of chloride diffusivity, the following conclusions can be drawn:

(1) The chloride content increased as the max load increased. At same max load, the chloride content at steel surface did not change regularly when cycles were 1, 5, and 10. However, when cycles were 20,

Table 7: Statistics of crack width variation before and after w-d cycles.

Code	Crack width	Measure points[1]	Crack evolution[2]		
			A[3]	B[4]	C[5]
B-0.4P1C	<0.1	15	9	4	2
	0.1–0.2	15	2	3	10
	≥0.2	0	0	0	0
B-0.4P5C	<0.1	12	8	2	2
	0.1–0.2	18	3	2	13
	≥0.2	0	0	0	0
B-0.4P10C	<0.1	13	10	2	1
	0.1–0.2	19	2	5	12
	≥0.2	0	0	0	0
B-0.4P20C	<0.1	18	12	3	3
	0.1–0.2	19	6	1	12
	≥0.2	2	0	0	2
B-0.5P1C	<0.1	15	12	2	1
	0.1–0.2	17	1	4	12
	≥0.2	4	0	0	4
B-0.5P5C	<0.1	11	6	2	3
	0.1–0.2	18	2	6	10
	≥0.2	4	0	0	4
B-0.5P10C	<0.1	15	10	3	2
	0.1–0.2	20	2	3	15
	≥0.2	4	0	0	4
B-0.5P20C	<0.1	14	6	4	4
	0.1–0.2	18	0	2	16
	≥0.2	7	0	0	7
B-0.6P1C	<0.1	26	15	6	5
	0.1–0.2	20	2	3	15
	≥0.2	8	0	0	8
B-0.6P5C	<0.1	19	8	6	5
	0.1–0.2	16	1	2	13
	≥0.2	8	0	0	8
B-0.6P10C	<0.1	25	16	6	3
	0.1–0.2	24	2	5	17
	≥0.2	10	0	0	10
B-0.6P20C	<0.1	17	12	2	3
	0.1–0.2	23	1	3	19
	≥0.2	15	0	0	15

Note. (1) Before w-d cycles; (2) after w-d cycles; (3) completely self-healing; (4) partly self-healing; (5) stable crack.

chloride content at steel surface was most. The max load had more influence on chloride content at steel surface than cycles.

(2) Chloride content at steel surface increased approximatively linearly as average crack width increased. The value of D_{avg} was significantly affected by crack distribution because D_{avg} in the positions with cracks or near cracks was higher than the uncracked positions. D_{avg} increased as crack width increased obviously when crack width was less than 0.11 mm whereas D_{avg} increased slowly as crack width increased when crack width exceeded 0.11 mm. The difference of D_{avg} between tension concrete and compression concrete was little in uncracked position.

(3) After cyclic loading and 240 wet-dry cycles of seawater, the residual yield load and ultimate load of RC beam specimens decreased as the max load amplitude and cycles increased. Compared with undamaged beam specimen, after 20 cycles of loading whose max load was $0.4P_u$, the yield load reduction increased from 10.4% to 26.8% and the ultimate load reduction increased from 7.9% to 21.5%. After 20 cycles of

loading whose max load was $0.6P_u$, the yield load reduction increased from 33.5% to 43.8% and the ultimate load reduction increased from 23.2% to 32.6%.

(4) Based on univariate analysis of variance, the max load had more adverse effect on yield load and ultimate load than cycles. The 20 cycles of loading had more adverse effect on yield load than 1, 5, and 10 cycles of loading.

Conflicts of Interest

The authors declare that there are no conflicts of interest regarding the publication of this paper.

Acknowledgments

This work is part of the projects financially supported by the Chinese National Natural Science Foundation (NSFC) Grant no. 51578031 and by the open topics of State Key Laboratory of Subtropical Architecture Science (SKLSAS) in South China University of Technology (2016ZA03). The authors gratefully acknowledge the financial support received from the NSFC and SKLSAS.

References

[1] O. G. Rodriguez and R. D. Hooton, "Influence of cracks on chloride ingress into concrete," *ACI Materials Journal*, vol. 100, no. 2, pp. 120–126, 2003.

[2] M. Şahmaran, "Effect of flexure induced transverse crack and self-healing on chloride diffusivity of reinforced mortar," *Journal of Materials Science*, vol. 42, no. 22, pp. 9131–9136, 2007.

[3] D. P. Bentz, E. J. Garboczi, Y. Lu, N. Martys, A. R. Sakulich, and W. J. Weiss, "Modeling of the influence of transverse cracking on chloride penetration into concrete," *Cement and Concrete Composites*, vol. 38, pp. 65–74, 2013.

[4] S. Y. Jang, B. S. Kim, and B. H. Oh, "Effect of crack width on chloride diffusion coefficients of concrete by steady-state migration tests," *Cement and Concrete Research*, vol. 41, no. 1, pp. 9–19, 2011.

[5] X. Y. Wang and L. N. Zhang, "Simulation of chloride diffusion in cracked concrete with different crack patterns," *Advances in Materials Science and Engineering*, vol. 2016, Article ID 1075452, 11 pages, 2016.

[6] Y. Li, X. Chen, L. Jin, and R. Zhang, "Experimental and numerical study on chloride transmission in cracked concrete," *Construction and Building Materials*, vol. 127, pp. 425–435, 2016.

[7] P. P. Win, M. Watanabe, and A. Machida, "Penetration profile of chloride ion in cracked reinforced concrete," *Cement and Concrete Research*, vol. 34, no. 7, pp. 1073–1079, 2004.

[8] C. Q. Li, "Initiation of chloride-induced reinforcement corrosion in concrete structural members—experimentation," *ACI Structural Journal*, vol. 98, no. 4, pp. 502–510, 2001.

[9] C. Q. Li, "Initiation of chloride-induced reinforcement corrosion in concrete structural members—prediction," *ACI Structural Journal*, vol. 99, no. 2, pp. 133–141, 2002.

[10] K. Park, H. Lee, and X. Wang, "Prediction of time-dependent chloride diffusion coefficients for slag-blended concrete," *Advances in Materials Science and Engineering*, vol. 2017, pp. 1–10, 2017.

[11] W.-J. Fan and X.-Y. Wang, "Prediction of chloride penetration into hardening concrete," *Advances in Materials Science and Engineering*, vol. 2015, Article ID 616980, 8 pages, 2015.

[12] S. H. Han, "Influence of diffusion coefficient on chloride ion penetration of concrete structure," *Construction and Building Materials*, vol. 21, no. 2, pp. 370–378, 2007.

[13] K. Li, C. Li, and Z. Chen, "Influential depth of moisture transport in concrete subject to drying-wetting cycles," *Cement and Concrete Composites*, vol. 31, no. 10, pp. 693–698, 2009.

[14] J. Wu, H. Li, Z. Wang, and J. Liu, "Transport model of chloride ions in concrete under loads and drying-wetting cycles," *Construction and Building Materials*, vol. 112, pp. 733–738, 2016.

[15] H. Ye, Y. Tian, N. Jin, X. Jin, and C. Fu, "Influence of cracking on chloride diffusivity and moisture influential depth in concrete subjected to simulated environmental conditions," *Construction and Building Materials*, vol. 47, no. 5, pp. 66–79, 2013.

[16] H. Ye, N. Jin, X. Jin, and C. Fu, "Model of chloride penetration into cracked concrete subject to drying-wetting cycles," *Construction and Building Materials*, vol. 36, pp. 259–269, 2012.

[17] B. Diao, J. Zhang, Y. Ye, and S. Cheng, "Effects of freeze-thaw cycles and seawater corrosion on the behavior of reinforced air-entrained concrete beams with persistent loads," *Journal of Cold Regions Engineering*, vol. 27, no. 1, pp. 44–53, 2013.

[18] B. Shen, Y. Ye, B. Diao, and X. Zheng, "Mechanical Performance and Chloride Diffusivity of Cracked RC Specimens Exposed to Freeze-Thaw Cycles and Intermittent Immersion in Seawater," *Advances in Materials Science and Engineering*, vol. 2016, Article ID 5973467, 2016.

[19] JTJ 270-98, Testing Code of Concrete for Port and Waterwog Engineering, China Communications Press, Beijing, China, 1998.

[20] P. Liu, Z. Yu, Z. Lu, Y. Chen, and X. Liu, "Predictive convection zone depth of chloride in concrete under chloride environment," *Cement and Concrete Composites*, vol. 72, pp. 257–267, 2016.

[21] G. de Vera, M. A. Climent, E. Viqueira, C. Antón, and C. Andrade, "A test method for measuring chloride diffusion coefficients through partially saturated concrete. Part II: The instantaneous plane source diffusion case with chloride binding consideration," *Cement and Concrete Research*, vol. 37, no. 5, pp. 714–724, 2007.

[22] M. A. Climent, G. De Vera, J. F. López, E. Viqueira, and C. Andrade, "A test method for measuring chloride diffusion coefficients through nonsaturated concrete: part I. The instantaneous plane source diffusion case," *Cement and Concrete Research*, vol. 32, no. 7, pp. 1113–1123, 2002.

[23] A. V. Saetta, R. V. Scotta, and R. V. Vitaliani, "Analysis of chloride diffusion into partially saturated concrete," *ACI Materials Journal*, vol. 90, no. 5, pp. 441–451, 1993.

[24] A. Ababneh, F. Benboudjema, and Y. Xi, "Chloride penetration in nonsaturated concrete," *Journal of Materials in Civil Engineering*, vol. 15, no. 2, pp. 183–191, 2003.

[25] L. P. Tang and L. O. Nilsson, "Chloride diffusivity in high strength concrete at different ages," *Nordic Concrete Research*, vol. 11, 1, pp. 162–171, 1992.

[26] The Life-365 Consortium III, The Silica Fume Association, "Life-365 v2.2.1 User's Manual," pp. 8-9, 2014, http://www.life-365.org/.

[27] CECS 220:2007, Standard for Durability Assessment of Concrete Structures, China Architectural and Building Press, Beijing, China, 2007.

[28] A. Djerbi, S. Bonnet, A. Khelidj, and V. Baroghel-bouny, "Influence of traversing crack on chloride diffusion into concrete," *Cement and Concrete Research*, vol. 38, no. 6, pp. 877–883, 2008.